ACS OMEGA

Open Access

http://pubs.acs.org/journal/acsodf

Article

Morphology and Emulsification of Poly(*N*-2-(methacryloyloxy) ethyl pyrrolidone)-*b*-poly(benzyl methacrylate) Assemblies by Polymerization-Induced Self-Assembly

Shuozhen Cheng, Jun Wang, Chunhui Li, Sixian He, Yashuang Liu, Yan Wang, Jinfeng Dong,* and Xuefeng Li*

Cite This: *ACS Omega* 2024, 9, 36917−36925

Read Online

ACCESS | Metrics & More | Article Recommendations | Supporting Information

ABSTRACT: In this work, a series of amphiphilic diblock copolymers poly(*N*-2-(methacryloyloxy) ethyl pyrrolidone)-*b*-poly(benzyl methacrylate) ($PNMP_m$-*b*-$PBzMA_n$) were developed by the dispersion polymerization method in ethanol. The polymerization-induced self-assembly (PISA) behaviors were studied systematically, and a comprehensive structure−property relationship was also established. Two distinct PISA tendencies were observed, which was mainly depended on the polymerization degree *m* of PNMP segment. When *m* is small such as 39 and 55, morphological transitions from spherical to vesicle-like assemblies via wormlike ones upon increasing *n* commonly happen regardless of the solid content. Alternatively, spherical assemblies became the sole morphology for $PNMP_{64}$-*b*-$PBzMA_n$ block copolymers because of the excellent solvophilicity of the $PNMP_{64}$ segment. Attributing to the amphiphilicity of $PNMP_m$-*b*-$PBzMA_n$ block copolymers, $PNMP_m$-*b*-$PBzMA_n$ assemblies by PISA are a type of excellent Pickering emulsifiers. These assemblies prefer to stabilize O/W Pickering emulsions as confirmed by the confocal laser scanning microscopy method, and the effects of polymerization degree of PBzMA segment or morphologies of $PNMP_m$-*b*-$PBzMA_n$ assemblies are finite.

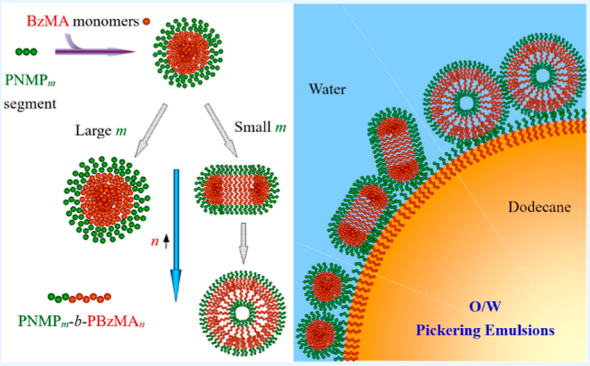

1. INTRODUCTION

In the past decades, studies on the development and self-assembly behaviors of polymeric amphiphiles become one of the most attractive topics because they show superiority to conventional surfactants in many physicochemical properties such as the lower dosage and higher efficiency, better stability and membrane intensity, and richer self-assembly behaviors.[1−3] These amphiphilic block copolymers are widely used in various fields including biotechnology, the development of functional materials, drug-controlled release systems, catalysis, and so forth.[1−6] It is well-known that inorganic solid particles with specific surface wettability are excellent emulsifiers to stabilize emulsions, namely, Pickering emulsions,[7,8] which show better stability than classic emulsions stabilized by surfactants. Recent studies show that assemblies of amphiphilic block copolymer can also be employed as Pickering emulsifiers,[9,10] and even multiple Pickering emulsions might be generated using a single block copolymer emulsifier,[11] which extensively enlarge the content and application potential of emulsions.[12−14] Attributing to the development of synthetic chemistry, the structures of amphiphilic block copolymers were diversified much. Although numerous synthetic methods of block copolymers were reported,[15−17] the polymerization-induced self-assembly (PISA) method is a shining star that accomplishes the development and preparation of block copolymer assemblies simultaneously.[18] Currently, the corresponding reaction requirement of PISA including the type of monomers, solvents, and the polymerization methods is experimentally studied well, and the major advantage and progress of PISA as well.[19−23]

The abundant self-assembly behavior is one of the most interesting characteristics of PISA, spherical, wormlike, and vesicle-like, and even other higher ordered assemblies can be generated.[24−28] The formation and growth of assemblies by PISA show high similarity to those of the conventional surfactants,[26] i.e., the morphological transitions from spherical to vesicle-like assemblies via wormlike ones are commonly reported through adjusting the polymerization degree of solvophobic segment in PISA systems, which also follow the well-known molecular packing parameter.[24,25,29] In addition, factors such as the polymerization degree, the alterable

Received: November 22, 2023
Revised: June 7, 2024
Accepted: July 30, 2024
Published: August 22, 2024

Scheme 1. Synthetic Route of $PNMP_m$-*b*-$PBzMA_n$ Block Copolymer Dispersions[a]

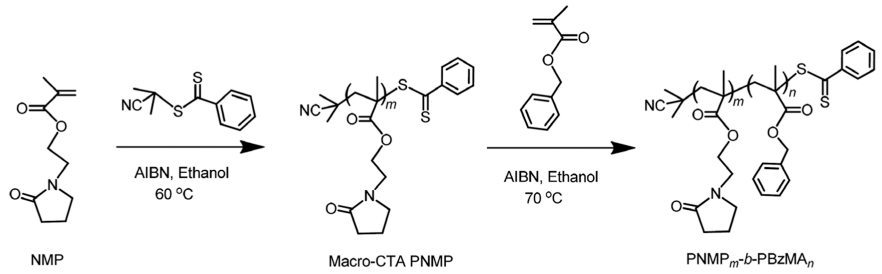

[a]The macromolecule chain-transfer reagent of PNMP (macro-CTA PNMP) was synthesized by the RAFT polymerization in ethanol at 60 °C first and then followed by a RAFT-mediated ethanol dispersion polymerization at 70 °C.

compression, solvation, and mobility of solvophobic segment, and the steric hindrance of solvophilic segment might also momentously affect the morphology of assemblies by PISA,[18,26,30,31] and thereby resulting in attractive indeterminacy during the PISA processes. For example, Armes and coworkers studied the PISA behaviors of PSMA-PBzMA diblock copolymers by employing the in situ small-angle X-ray scattering (SAXS) technique.[32] Although spherical, wormlike, and vesicle-like nano-objects were formed for $PSMA_{13}$-$PBzMA_x$ series diblock copolymers by the gradual growth mechanism. However, spheres became the sole morphology in the $PSMA_{31}$-$PBzMA_x$ and $PSMA_{18}$-$PBzMA_x$ dispersions even increasing x to 2000, in which the excellent solvophilicity of the PSMA segment with the larger polymerization degree was critical.

Our group has reported some pyrrolidone-based amphiphilic diblock copolymers developed by the RAFT method, which not only show abundant self-assembly behaviors in the selected solvents but also display interesting stimuli responses.[33−35] For example, poly(*N*-(2-methacrylaoyxyethyl)-pyrrolidone)-*b*-poly(methyl methacrylate) (PNMP-*b*-PMMA) could form thermal-response organogels in isopropanol because of the disassembly of 3D micellar networks at the higher temperature.[35] Similar amphiphilic copolymers were alternatively prepared by the PISA method by other groups, and rich self-assembly behaviors were observed.[36,37] Recently, a new family of pyrrolidone-based amphiphilic diblock copolymers, poly(*N*-2-(methacryloyloxy) ethyl pyrrolidone)-*b*-poly(benzyl methacrylate) (PNMP-*b*-PBzMA), were reported. The morphologies of $PNMP_{50}$-*b*-$PBzMA_n$ assemblies show gradual transition from spherical to vesicle-like assemblies via wormlike ones.[38] However, a comprehensive illustration about the structure−property relationship of PNMP-*b*-PBzMA diblock copolymers is still unknown.

In this work, $PNMP_m$-*b*-$PBzMA_n$ amphiphilic diblock copolymers were synthesized by the reversible addition−fragmentation chain transfer (RAFT) dispersion polymerization method in ethanol, and their PISA behaviors were studied systematically by various techniques including dynamic light scattering (DLS), transmission electron microscopy (TEM), and scanning electron microscopy (SEM) measurements. To establish the structure−property relationship of $PNMP_m$-*b*-$PBzMA_n$ diblock copolymers, factors such as the polymerization degree m and n of PNMP and PBzMA segments, respectively, and the solid content on the morphologies of assemblies were considered carefully. Moreover, the emulsification of $PNMP_m$-*b*-$PBzMA_n$ assemblies by PISA was evaluated in detail. The comprehensive physiochemical properties of $PNMP_m$-*b*-$PBzMA_n$ diblock copolymers provide solid basics for their application potential in the related fields fundamentally.

2. EXPERIMENTAL SECTION

2.1. Materials. 2-Cyanopropyl-2-dithiobenzoate (CPDB) was synthesized according to the reported method.[27] 2, 2′-Azobis(isobutyronitrile) (AIBN, 99%) was purchased from Shanghai HATECH Co. Ltd. and recrystallized in ethanol twice. *N*-hydroxyethyl pyrrolidone and benzyl methacrylate (BzMA, 98%) were purchased from TCI Development Co., Ltd. (Shanghai). Methacryloyl chloride (98%, Shanghai HATECH Co. Ltd.) was distilled under reduced pressure before use. Dimethylformamide (DMF, 99%, Shanghai HATECH Co. Ltd.) was distilled under reduced pressure, which was mixed with 0.05 mol·L^{-1} $NaNO_3$ (99%, Shanghai HATECH Co. Ltd.) and then filtered on 0.2 μm polytetrafluoroethylene filters for gel permeation chromatography (GPC). Nile red (99%) was obtained from Sigma-Aldrich. All other solvents and reagents were purchased from commercial sources and were used as received.

2.2. Synthesis of $PNMP_m$-*b*-$PBzMA_n$ Diblock Copolymer Dispersions. $PNMP_m$-*b*-$PBzMA_n$ block copolymer dispersions were synthesized according to the following procedure (Scheme 1):[38]

2.2.1. Synthesis of N-2-(Methacryloyloxy)ethyl Pyrrolidone (NMP) Monomer. NMP monomer was synthesized and purified by the previous reported methods,[35] yield: 67%. ^{1}H NMR (ppm, $CDCl_3$): 6.11 and 5.60 (2H, CH_2═CCH_3), 4.29 (2H, $COOCH_2CH_2$), 3.6 (2H, $COOCH_2CH_2$), 3.5 (2H, $NCOCH_2CH_2$ CH_2 in the pyrrolidone ring), 2.42 (2H, $NCOCH_2CH_2CH_2$ in the pyrrolidone ring), 2.05 (2H, $NCOCH_2CH_2CH_2$ in the pyrrolidone ring), and 1.95 (3H, CH_2═$CHCH_3$).

2.2.2. Synthesis of Macro-CTA PNMP. The synthetic route of macro-CTA PNMP was reported in detail elsewhere,[35] and the representative formulation of macro-CTA $PNMP_{39}$ was described as following: NMP (40.0 g, 203.04 mmol), CPDB (1.07 g, 4.84 mmol), AIBN (0.26 g, 1.58 mmol), and CH_3CH_2OH (80 mL) were charged in a 200 mL Schlenk flask capped with rubber septa. Subsequently, the homogeneous solution was deoxygenated by purging with highly pure nitrogen gas for 30 min and then reacted at 60 °C for 10 h under stirring in a thermostatic oil bath. The monomer conversion at 93% was determined by ^{1}H NMR analysis employing the internal standard of 1, 3, 5-trioxane. The crude product was diluted by dichloromethane and then poured into diethyl ether to precipitate at least twice. The final product was dried in a vacuum oven at 45 °C to give a pink powder. The mean degree of polymerization was calculated using ^{1}H NMR

https://doi.org/10.1021/acsomega.3c09315
ACS Omega 2024, 9, 36917−36925

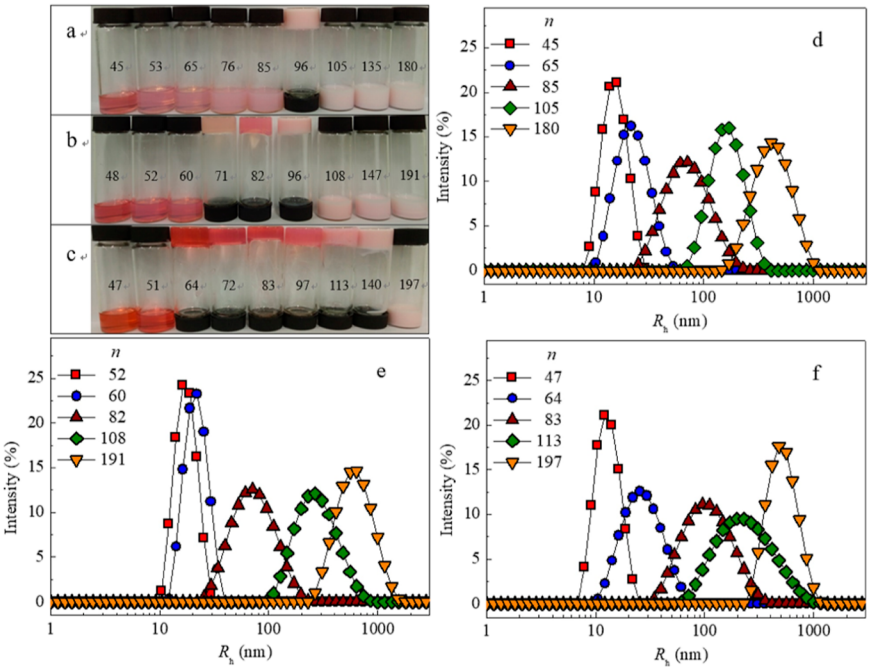

Figure 1. Appearance of $PNMP_{39}$-*b*-$PBzMA_n$ dispersions prepared by PISA at the solid content of 10 (a), 20 (b), and 30 wt % (c) in ethanol at 70 °C, and the inset number represents the corresponding polymerization degree *n* of PBzMA segment. Typical size distributions of them prepared at solid contents of 10 (d), 20 (e), and 30 wt % (f).

to be 39 by comparing the integrated aromatic proton signals of CPDB at 7.3−8.0 ppm to that of the methylene carbonyl signals at 4.06 ppm. DMF GPC analysis indicated the M_n of 7064 g·mol^{-1} and a M_w/M_n of 1.01 [vs a series of near-monodisperse poly(methyl methacrylate) calibration standards]. Macro-CTA $PNMP_{55}$ and macro-CTA $PNMP_{64}$ were synthesized by the same routes, and detailed structural information is provided in Figure S1 and Table S1.

2.2.3. Synthesis of $PNMP_m$-b-$PBzMA_n$ Diblock Copolymer Dispersions in Ethanol. A typical synthesis of $PNMP_{39}$-*b*-$PBzMA_{115}$ diblock copolymer dispersion at the solid content of 20 wt % was described as following: macro-CTA $PNMP_{39}$ (0.250 g; 0.0325 mmol), BzMA (0.658 g; 3.74 mmol; target *n* = 115), and AIBN (1.066 mg; 6.50 μmol; dissolved at 0.1% w/w in ethanol; CTA/AIBN molar ratio = 5.0) were dissolved in ethanol (2.748 g) in a 15 mL Schlenk flask capped with rubber septa. Subsequently, the homogeneous solution was deoxygenated by purging with highly pure nitrogen gas for 30 min and then reacted at 70 °C for 24 h under stirring in a thermostatic oil bath. The final monomer conversion was determined by ^{1}H NMR spectroscopy analysis by integrating the PBzMA peak (CH) at 5.0−4.7 ppm to the vinyl peaks (CH_2) of BzMA monomers at 5.17 ppm. The final reaction dispersion was diluted approximately 10-fold in $CDCl_3$ and showed a conversion of BzMA monomers about 93% (Figure S2). DMF GPC analysis indicated a M_n of 24,430 g·mol^{-1} and M_w/M_n of 1.02. The kinetic results (Figure S3a,c) show that the conversion of BzMA monomers increases gently at the initial 5 h and then follows a rapid and linear increase process because of the formation of monomer-swollen copolymer particles during the micellar nucleation process.[38] The linear evolution of molecular weight with conversion indicates a well-controlled pseudoliving RAFT polymerization (Figure S3b,d).

Other $PNMP_m$-*b*-$PBzMA_n$ diblock copolymer dispersions were synthesized by the same routes at the solid content of 10, 15, 20, 25, and 30 wt %, and totally 56 different $PNMP_m$-*b*-$PBzMA_n$ diblock copolymer dispersions were developed. All $PNMP_m$-*b*-$PBzMA_n$ diblock copolymers were characterized by GPC and ^{1}H NMR systematically, and the detailed molecular information is summarized in Figure S4 and Table S2.

2.3. Characterization of $PNMP_m$-*b*-$PBzMA_n$ Diblock Copolymers. ^{1}H NMR spectra were recorded on a 400 MHz Bruker-BioSpin spectrometer using $CDCl_3$. GPC measurements were performed at 35 °C using DMF (containing 0.05 M $NaNO_3$) as the eluent at a flow rate of 1.0 mL·min^{-1}. The column set consisted of two MZ-SD *plus* 5 μm columns (500 Å and linear); Wyatt Optilab DSP Interferometric refractometer and Wyatt DAWN EOS multiangle laser light scattering detector with a helium−neon laser light source (λ = 685 nm), K5-flow cell, and a broad range of scattering angle from 45 to 160° were employed. The molecular weight and polydispersity data were determined using the Wyatt ASTRA software package. The refractive index increment of the polymer solution (dn/dc) was measured using an Optilab DSP refractometer at a wavelength of 685 nm.

2.4. Preparation of $PNMP_m$-*b*-$PBzMA_n$ Assembly-Stabilized Emulsions. The aqueous dispersions of $PNMP_m$-*b*-$PBzMA_n$ assemblies were obtained directly by diluting the corresponding PISA solutions under stirring until homogeneous. All emulsions were prepared using an IKA Ultra-Turrax T-18 homogenizer equipped with a 10 mm dispersing tool, in which the mixture of dodecane and block copolymer micelle solution with the total volume of 2 mL was homogenized for 3 min at 25 °C. The oil phase containing Nile red and the fluorescent probe-solubilized $PNMP_m$-*b*-$PBzMA_n$ aqueous dispersions were prepared according to the reported procedure.[9]

2.5. Characterization of $PNMP_m$-*b*-$PBzMA_n$ Diblock Copolymer Assemblies. DLS was performed on a Zetasizer ZEN 3600 (Malvern, U.K.) with a 173° back scattering angle and He−Ne laser (λ = 633 nm) at 25 °C. Each dispersion was diluted by ethanol into 0.20 wt % before measurements.

https://doi.org/10.1021/acsomega.3c09315
ACS Omega 2024, 9, 36917−36925

TEM measurements were conducted with a JEOL JEM-100CXII transmission electron microscope at an accelerating voltage of 120 kV. Samples for TEM observation were prepared as following: the diluted dispersions (0.20 wt % in ethanol, 10.0 μL) were dropped to the carbon-coated grids, and the excess solution was blotted with filter paper after 1 min and then dried under ambient conditions.

SEM observations were performed on an FEI Zeiss Sigma SEM. The samples for SEM observations were prepared by casting a drop of diluted dispersion (0.20 wt % in ethanol, 5.0 μL) on a polished silicon wafer, followed by drying under ambient conditions, and gold was coated on the sample surface with 80 s sputtering time and 30 mA current.

Light microscopy images were performed on an Olympus BX 51 microscopy (Japan). Fluorescence microscope images of emulsion droplets were recorded with the Ultraview Vox spinning disc confocal system (PerkinElmer) equipped with a Yokogawa CSU-X1 spinning disc head and EMCCD camera (Hamamatsu C9100-13) and coupled with a Nikon Ti-E microscope. Confocal image acquisition and analysis were performed with Volocity software (PerkinElmer) according to the reported procedure.[9]

3. RESULTS AND DISCUSSION

3.1. Effect of Polymerization Degree *n* of PBzMA Segment. Figure 1a–c shows the macro-appearance of $PNMP_{39}$-*b*-$PBzMA_n$ diblock copolymer assemblies synthesized at the solid contents of 10, 20, and 30 wt %, respectively. Each series of samples shows a similar transition tendency, transition from optical transparency to opaque gradually via a viscous intermediate state upon increasing *n*, indicating the microstructural change of assemblies. For example, the dispersion of $PNMP_{39}$-*b*-$PBzMA_{96}$ (Figure 1a) can be inverted without any perturbation; however, the viscous region would be enlarged at the higher solid content. Viscosity results (Figure S5) show that the viscosity of $PNMP_{39}$-*b*-$PBzMA_n$ dispersions with a small or large *n*, i.e., $PNMP_{39}$-*b*-$PBzMA_{45}$ and $PNMP_{39}$-*b*-$PBzMA_{180}$, is very low (~1 mPa·s). In contrast, those of $PNMP_{39}$-*b*-$PBzMA_{85}$, $PNMP_{39}$-*b*-$PBzMA_{96}$, and $PNMP_{39}$-*b*-$PBzMA_{105}$ become very high, showing typical shear-thinning behaviors as non-Newton fluids. These characters of amphiphilic homologues often suggest the morphological transition of assemblies from spherical to vesicle-like via wormlike shapes.[29,31]

Figure 1d–f shows the corresponding size distributions of diluted $PNMP_{39}$-*b*-$PBzMA_n$ dispersions at different solid contents, which exhibit similarity. The radius of assemblies (R_h) is increased from tens to hundreds of nanometers upon increasing *n*, which is consistent with the transition from spherical to vesicle-like via wormlike assemblies mentioned above. To make clear evidence, samples were studied using the electric microscopy techniques. Figure 2 shows the representative TEM and SEM images of $PNMP_{39}$-*b*-$PBzMA_n$ assemblies generated at 20 wt %. Spherical assemblies are formed in the $PNMP_{39}$-*b*-$PBzMA_{52}$ dispersion (Figure 2a). Alternatively, linear, branched, and even entangled wormlike assemblies of $PNMP_{39}$-*b*-$PBzMA_{82}$ become the majority (Figure 2b). For $PNMP_{39}$-*b*-$PBzMA_{108}$, both wormlike and vesicle-like assemblies are formed as observed (Figure 2c). In addition, the jellyfish assemblies (the inset image in Figure 2c) are the intermediate states of assemblies, which were widely observed in similar PISA systems during the wormlike to vesicle-like morphology transition process.[31,39,40] Further increasing *n* to

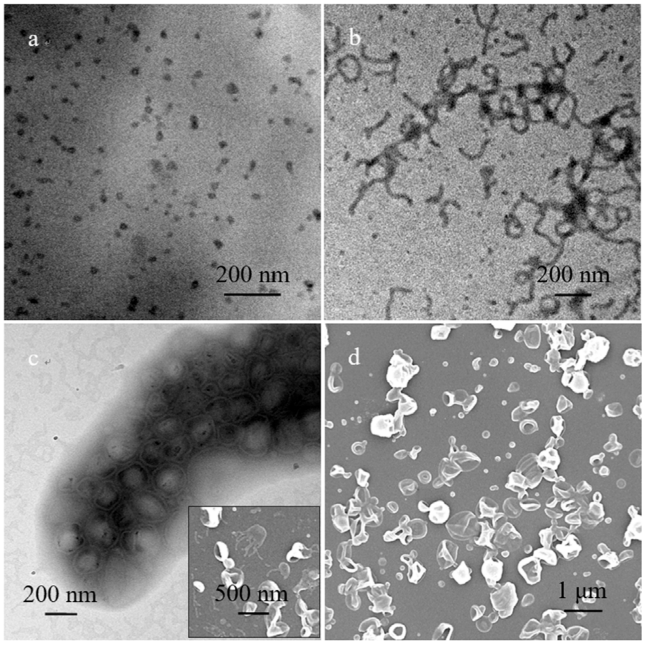

Figure 2. TEM images of $PNMP_{39}$-*b*-$PBzMA_{52}$ (a), $PNMP_{39}$-*b*-$PBzMA_{82}$ (b), and $PNMP_{39}$-*b*-$PBzMA_{108}$ (c), and SEM image of $PNMP_{39}$-*b*-$PBzMA_{191}$ (d). Inset image in (c) is the corresponding SEM image of $PNMP_{39}$-*b*-$PBzMA_{108}$.

191, mainly vesicles are visible (Figure 2d). Undoubtedly, the results confirm the gradual morphological transition of assemblies from spherical to vesicle-like via wormlike shapes.[41,42]

Similar morphological transitions of assemblies also happened for $PNMP_{39}$-*b*-$PBzMA_n$ dispersions synthesized at other solid content (Figures S6 and S7). Figure 3 illustrates the morphological dependence between the polymerization degree of the PBzMA segment and the solid content of $PNMP_{39}$-*b*-$PBzMA_n$ diblock copolymer dispersions. Obviously, the morphologies of $PNMP_{39}$-*b*-$PBzMA_n$ assemblies are mainly depended on *n*, and the solid content affects a little. The transitions of aggregates from spherical to vesicle-like

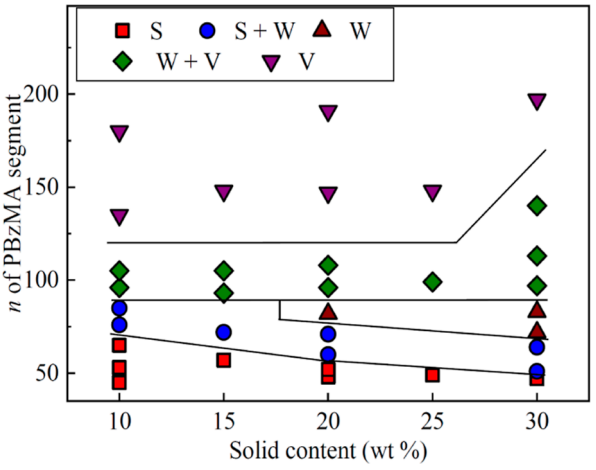

Figure 3. Dependence of aggregates on the polymerization degree of the PBzMA segment and the solid content in the $PNMP_{39}$-*b*-$PBzMA_n$ diblock copolymer dispersions prepared by PISA in ethanol at 70 °C. S, W, and V represent spherical, wormlike, and vesicle-like assemblies, respectively.

https://doi.org/10.1021/acsomega.3c09315
ACS Omega 2024, 9, 36917–36925

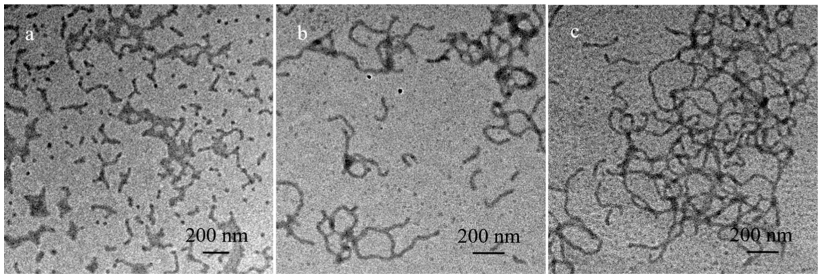

Figure 4. TEM images of $PNMP_{39}$-*b*-$PBzMA_{85}$ (a), $PNMP_{39}$-*b*-$PBzMA_{82}$ (b), and $PNMP_{39}$-*b*-$PBzMA_{83}$ (c) prepared at 10, 20, and 30 wt % solid content, respectively.

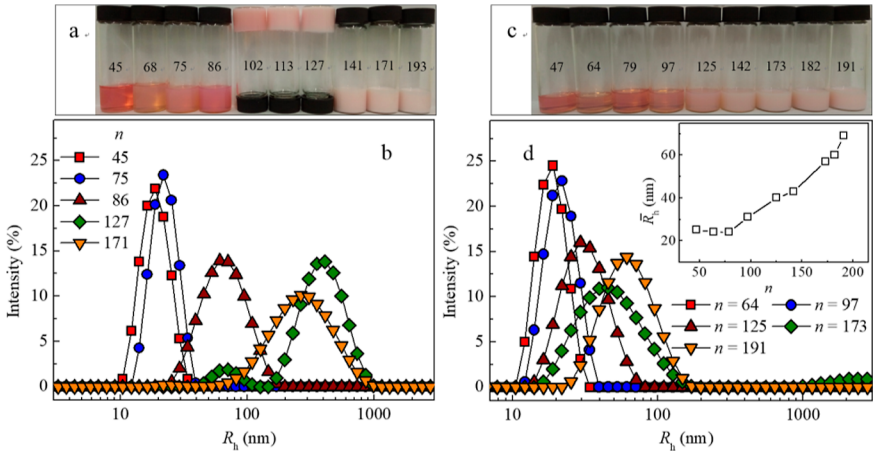

Figure 5. Appearance and typical size distribution of $PNMP_{55}$-*b*-$PBzMA_n$ (a,b) and $PNMP_{64}$-*b*-$PBzMA_n$ (c,d) diblock copolymer dispersions prepared by PISA at the solid content of 20 wt % in ethanol at 70 °C, and the inset image in (d) represents the dependence of averaged size on *n*.

assemblies via wormlike ones along with the increase of *n* are the major characteristic. That is to say, the increased solvophobic PBzMA segment benefits the formation of assemblies with larger size, which also follows the molecular parameter theory well.[29]

We also noticed the enlarged viscous region of $PNMP_{39}$-*b*-$PBzMA_n$ dispersions at the higher solid content (Figure 1a–c), and wormlike assemblies were often formed in these dispersions. To clarify the microstructural difference caused by the solid content, assemblies of $PNMP_{39}$-*b*-$PBzMA_n$ block copolymers with *n* around 83 ± 2 formed at different solid content were studied and are shown in Figure 4. The morphology of $PNMP_{39}$-*b*-$PBzMA_{85}$ assemblies prepared at the solid content of 10 wt % is short rods with the size of about several hundred of nanometers. For the $PNMP_{39}$-*b*-$PBzMA_{82}$ dispersion synthesized at 20 wt % solid content, linear, branched, and entangled wormlike shapes are formed. Once the solid content was increased to 30 wt %, very long and entangled wormlike assemblies of $PNMP_{39}$-*b*-$PBzMA_{83}$ about several micrometers became majority. Since assemblies with different morphologies by PISA were often resulted from the initially formed spheres by agglomeration, destruction, and recombination processes, as confirmed by SAXS and TEM techniques.[26,31,32] The higher solid content is certainly beneficial to the formation of wormlike assemblies with longer length. Thus, the enlarged viscous region can be attributed to the formation of wormlike assemblies with longer length.

3.2. Effect of Polymerization Degree *m* of PNMP Segment. Figure 5 shows the macro-appearance and size distribution of $PNMP_{55}$-*b*-$PBzMA_n$ and $PNMP_{64}$-*b*-$PBzMA_n$ series block copolymers, which were developed at 20 wt % solid content. Nearly no difference can be distinguished from the appearance of $PNMP_{55}$-*b*-$PBzMA_n$ (Figure 5a) and $PNMP_{39}$-*b*-$PBzMA_n$ (Figure 1b). Both undergo similar transitions from optical transparency to turbidity via a viscous region along with the enlarged *n*, and the average sizes of assemblies are increased from about 20 nm to hundreds of nanometers (Figures 1e and 5b). TEM and SEM images of $PNMP_{55}$-*b*-$PBzMA_n$ dispersions (Figure 6) show the morphological transition from spherical to vesicle-like assemblies via wormlike ones, confirming the self-assembly similarity between $PNMP_{55}$-*b*-$PBzMA_n$ and $PNMP_{39}$-*b*-$PBzMA_n$.

However, the behaviors of $PNMP_{64}$-*b*-$PBzMA_n$ series become significantly different so that all dispersions keep thinning states except the increased turbidity (Figure 5c). DLS results (Figure 5d) show that the average radius R_h of assemblies is about 25 nm when *n* is below 80, whereas it increases linearly upon further increasing *n* as observed in other PISA systems.[32,43] TEM images of $PNMP_{64}$-*b*-$PBzMA_{64}$ (Figure 7a), $PNMP_{64}$-*b*-$PBzMA_{125}$ (Figure 7b), and $PNMP_{64}$-*b*-$PBzMA_{173}$ (Figure 7c) show that only spherical assemblies are formed. This suggests that the morphologies of $PNMP_{64}$-*b*-$PBzMA_n$ assemblies are independent of *n*, and the increased turbidity is caused by the enlarged size. Interestingly, some irregular spheres such as the spindle-like (inset image in Figure 7b) and triangle (inset image in Figure 7c) ones are also distinguishable, suggesting that larger spherical assemblies should result from the fusion of initially formed ones.

The general self-assembly behaviors of $PNMP_m$-*b*-$PBzMA_n$ block copolymers prepared at the constant solid content of 20 wt % can be preliminary illustrated by Figure 8 based on the relationship between *m* and *n*. The diagram presented here

https://doi.org/10.1021/acsomega.3c09315
ACS Omega 2024, 9, 36917−36925

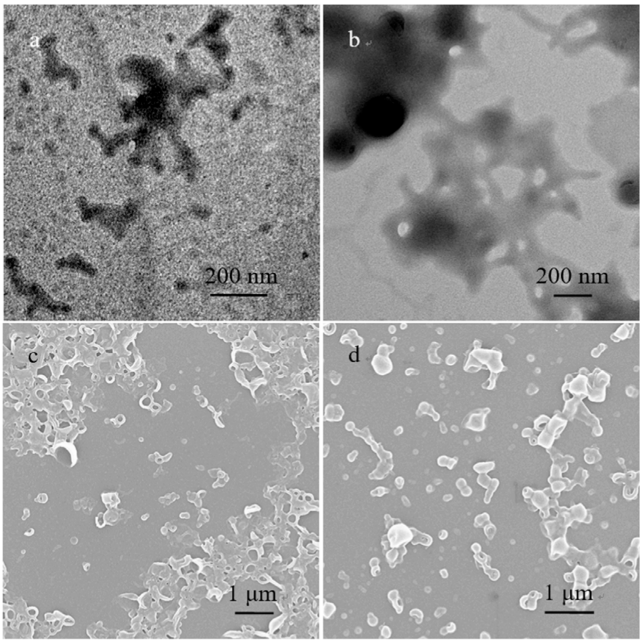

Figure 6. TEM images of $PNMP_{55}$-*b*-$PBzMA_{86}$ (a), $PNMP_{55}$-*b*-$PBzMA_{127}$ (b), and SEM images of $PNMP_{55}$-*b*-$PBzMA_{141}$ (c) and $PNMP_{55}$-*b*-$PBzMA_{193}$ (d) diblock copolymer dispersions synthesized at the solid content of 20 wt % in ethanol at 70 °C.

strongly suggests two distinct tendencies. When *m* is small (<55), the morphological transitions from spherical to vesicle-like assemblies via wormlike ones are happened upon increasing *n*. When *m* arrives at 64, only spherical assemblies are generated regardless of *n*. Similar dependences of the self-assembly behaviors on the polymerization degree of solvophilic segment are widely reported in PISA systems previously.[26,31,32,43−45] The processes relate to the altered assembly manner of assemblies from kinetically controlled to thermodynamically controlled during the PISA process because the PNMP segment with larger *m* would increase the solubility and solvophilicity of $PNMP_m$-*b*-$PBzMA_n$ block copolymers, which form spherical micelles spontaneously.[38]

3.3. Emulsification of $PNMP_m$-*b*-$PBzMA_n$ Assemblies.

The emulsification of $PNMP_{39}$-*b*-$PBzMA_n$ assemblies was evaluated in the dodecane/water systems, in which $PNMP_{39}$-*b*-$PBzMA_n$ aqueous dispersions were obtained through diluting 30 wt % PISA dispersions by water. During the emulsification processes, the concentration of $PNMP_{39}$-*b*-$PBzMA_n$ ($c_{Emulsifier}$), the oil/water volume ratio (V_O/V_W), and the shear rate were kept constant at 0.5 wt %, 1/1, and 12,000 rpm, respectively. Generally, stable and gel-like O/W emulsions can be formed at

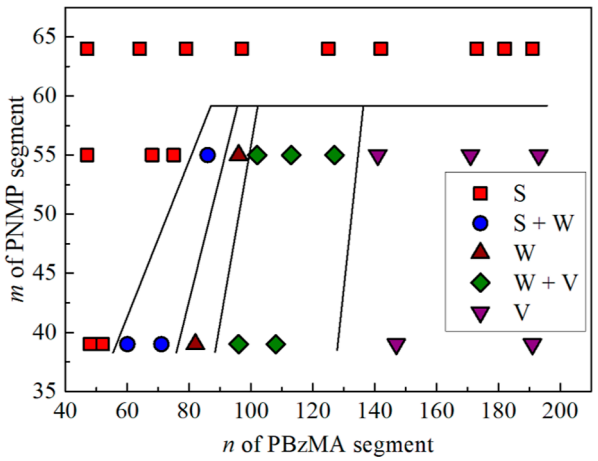

Figure 8. Dependence of self-assemblies on the polymerization degree of PNMP and PBzMA segments prepared at the constant solid content of 20 wt % by PISA in ethanol at 70 °C. S, W, and V represent spherical, wormlike, and vesicle-like assemblies, respectively.

the top phase for all $PNMP_{39}$-*b*-$PBzMA_n$ emulsifiers. Light microscopy images show that $PNMP_{39}$-*b*-$PBzMA_n$-stabilized emulsions were well-distributed, and no significant difference can be distinguished with the average size of about tens of micrometers (Figure S8). The original morphologies of $PNMP_{39}$-*b*-$PBzMA_{47}$, $PNMP_{39}$-*b*-$PBzMA_{83}$, and $PNMP_{39}$-*b*-$PBzMA_{197}$ are spherical, wormlike, and vesicle-like, respectively, emulsions stabilized by them were studied further by the confocal laser scanning microscopy (CLSM) method (Figure 9a−c). Since Nile red was dissolved in dodecane before emulsification, the fluorescent and dispersed droplets evidence the formation of O/W emulsions. This also suggests that the type of emulsion is independent of the polymerization degree *n* of the PBzMA segment. In other words, there is no immediate relationship between the type of emulsion and the morphology of assemblies as reported previously,[11] and the dominant hydrophilicity of $PNMP_{39}$-*b*-$PBzMA_n$ assemblies might be the major cause.

To lighten the interfacial layer of emulsions, $PNMP_{39}$-*b*-$PBzMA_n$ assemblies stabilized emulsions were also studied by the developed CLSM method,[9] in which Nile red was solubilized in $PNMP_{39}$-*b*-$PBzMA_n$ assemblies before emulsification (Figure 9d,e). In this case, the fluorescence mainly came from the oil/water interfacial layers instead of dispersed dodecane droplets (Figure 9a−c). The remarkable interfacial fluorescence of emulsion droplets confirms that $PNMP_{39}$-*b*-$PBzMA_n$ assemblies must remain and participate in the emulsification, suggesting the formation of Pickering emul-

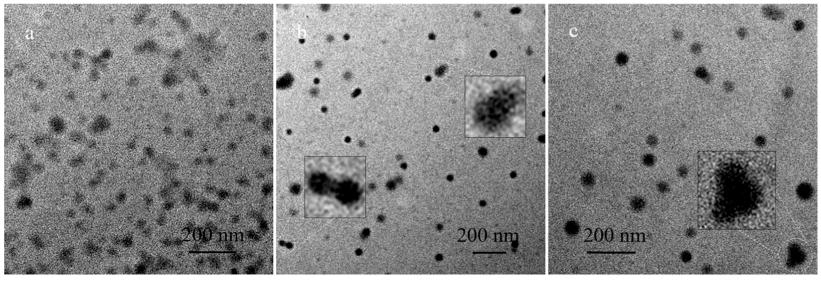

Figure 7. TEM images of $PNMP_{64}$-*b*-$PBzMA_{64}$ (a), $PNMP_{64}$-*b*-$PBzMA_{125}$ (b), and $PNMP_{64}$-*b*-$PBzMA_{173}$ (c) dispersions prepared at the solid content of 20 wt % in ethanol at 70 °C. The inset images correspond to the area signed by the circle in (b,c), respectively.

https://doi.org/10.1021/acsomega.3c09315
ACS Omega 2024, 9, 36917−36925

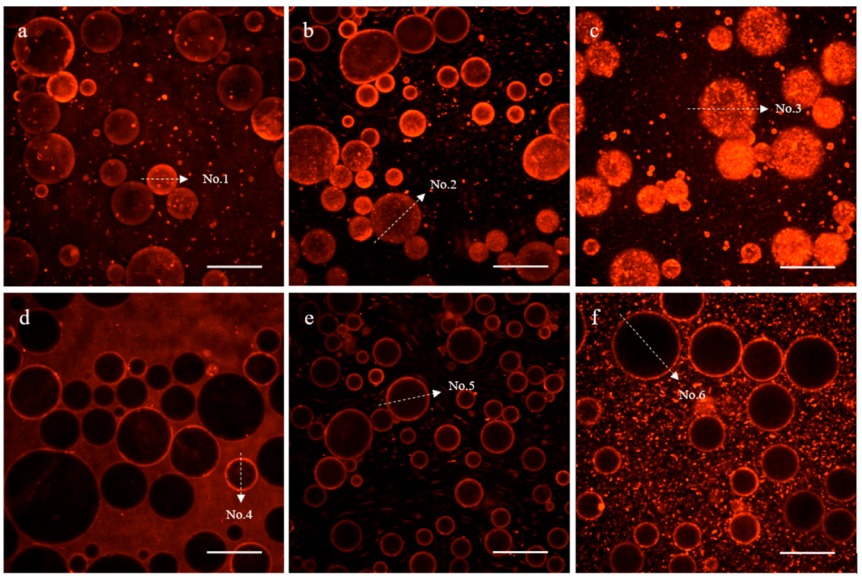

Figure 9. CLSM images of emulsions stabilized by $PNMP_{39}$-*b*-$PBzMA_{47}$ (a,d), $PNMP_{39}$-*b*-$PBzMA_{83}$ (b,e), and $PNMP_{39}$-*b*-$PBzMA_{197}$ (c,f) assemblies, respectively. Bars: 100 μm.

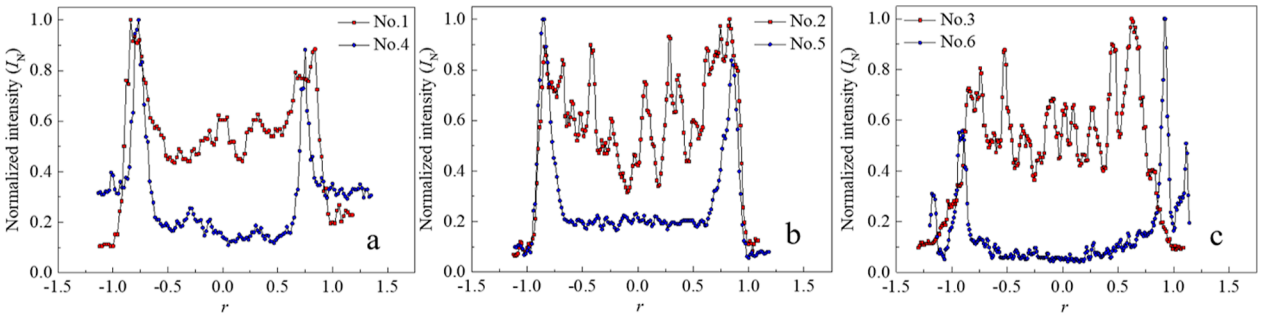

Figure 10. Normalized fluorescent intensity (I_N) vs the normalized radius (r) curves of emulsion droplets along the signed direction.

sions. Otherwise, the interfacial layer should be indistinguishable, along with the disassembly of $PNMP_{39}$-*b*-$PBzMA_n$ assemblies. Figure 10 shows the normalized fluorescent intensity (I_N) versus the normalized radius (r) curves of the representative emulsion droplets from no. 1 to no. 6 along the singed direction, where r and I_N are the data divided by the radius of the emulsion droplet and the maximum fluorescent intensity along the signed direction, respectively.[10] If Nile red was dissolved in dodecane, the fluorescent intensity of the inner oil droplet was very strong, whereas it was weakened remarkably, and the interfacial fluorescence became dominant once Nile red was alternatively solubilized in assemblies. The strong interfacial fluorescence certainly confirms the presence of $PNMP_m$-*b*-$PBzMA_n$ assemblies at the oil/water interfaces of emulsions, indicating the formation of Pickering emulsions rather than normal emulsions. Thus, $PNMP_m$-*b*-$PBzMA_n$ assemblies developed by PISA are excellent Pickering emulsifiers.

4. CONCLUSIONS

In summary, this work developed a series of $PNMP_m$-*b*-$PBzMA_n$ diblock copolymers by the RAFT dispersion polymerization method, and the corresponding PISA behaviors of them were studied in detail. Morphologies of $PNMP_m$-*b*-$PBzMA_n$ assemblies were characterized systematically and established a comprehensive structure−property relationship. Accordingly, the morphological dependence of $PNMP_m$-*b*-$PBzMA_n$ assemblies on the solid content and the polymerization degree of PNMP and PBzMA segments were clarified. Generally, the solid content affects the self-assembly behaviors a little, whereas the effect of the polymerization degree of the PBzMA segment is significant. In the $PNMP_{39}$-*b*-$PBzMA_n$ and $PNMP_{55}$-*b*-$PBzMA_n$ series, morphological transitions from spherical to vesicle-like via wormlike assemblies are commonly happened upon increasing n, resulting from the gradual fusion of initially formed spherical assemblies. Alternatively, the spherical shape became the major morphology of assemblies for $PNMP_{64}$-*b*-$PBzMA_n$ series block copolymers because of the excellent solvophilicity of the $PNMP_{64}$ segment. We also noticed the excellent emulsification of $PNMP_m$-*b*-$PBzMA_n$ assemblies, which preferred to stabilize O/W Pickering emulsions as confirmed by the CLSM method, in which the polymerization degree of the PBzMA segment or the morphologies of $PNMP_m$-*b*-$PBzMA_n$ assemblies is finite. Thus, $PNMP_m$-*b*-$PBzMA_n$ might shed application potential in fields of drug-controlled release, the development of nano/micro-materials as a template, the enhancement of crude oil recovery, and so forth.

https://doi.org/10.1021/acsomega.3c09315
ACS Omega 2024, 9, 36917−36925

■ ASSOCIATED CONTENT

Supporting Information

The Supporting Information is available free of charge at https://pubs.acs.org/doi/10.1021/acsomega.3c09315.

Molecular information and methods for the calculation of the polymerization degree m and n of macromolecule chain-transfer reagent of macro-CTA $PNMP_m$ and $PNMP_m$-b-$PBzMA_n$ block copolymers from GPC and ^1H NMR results, rheological responses and morphologies of $PNMP_{39}$-b-$PBzMA_n$ series block copolymer dispersions prepared at different solid contents, and light microscopy images of emulsions stabilized by $PNMP_{39}$-b-$PBzMA_n$ block copolymers (PDF)

■ AUTHOR INFORMATION

Corresponding Authors

Jinfeng Dong − *College of Chemistry and Molecular Sciences, Wuhan University, Wuhan 430072, P. R. China*; Email: jfdong@whu.edu.cn

Xuefeng Li − *College of Chemistry and Molecular Sciences, Wuhan University, Wuhan 430072, P. R. China*; orcid.org/0000-0002-7277-0130; Email: lixuefeng@whu.edu.cn

Authors

Shuozhen Cheng − *College of Chemistry and Molecular Sciences, Wuhan University, Wuhan 430072, P. R. China; Chemistry Metrology Division, Hubei Institute of Measurement and Testing Technology, Wuhan 430200, P. R. China*

Jun Wang − *Oil & Gas Technology Research Institute, Changqing Oilfield Company, Xi'an 710018, China; National Engineering Laboratory for Exploration and Development of Low-Permeable Oil and Gas Fields, PetroChina Changqing Oilfield Company, Xi'an 710018, China*

Chunhui Li − *College of Chemistry and Molecular Sciences, Wuhan University, Wuhan 430072, P. R. China*

Sixian He − *Oil & Gas Technology Research Institute, Changqing Oilfield Company, Xi'an 710018, China; National Engineering Laboratory for Exploration and Development of Low-Permeable Oil and Gas Fields, PetroChina Changqing Oilfield Company, Xi'an 710018, China*

Yashuang Liu − *College of Chemistry and Molecular Sciences, Wuhan University, Wuhan 430072, P. R. China*

Yan Wang − *Oil & Gas Technology Research Institute, Changqing Oilfield Company, Xi'an 710018, China; National Engineering Laboratory for Exploration and Development of Low-Permeable Oil and Gas Fields, PetroChina Changqing Oilfield Company, Xi'an 710018, China*

Complete contact information is available at: https://pubs.acs.org/10.1021/acsomega.3c09315

Notes

The authors declare no competing financial interest.

■ ACKNOWLEDGMENTS

This work was supported by the National Natural Science Foundation of China (NSFC 22072109 and 21773174). We are grateful to the Core Facility of Wuhan University for the electron microscopy and CLSM measurements.

■ REFERENCES

(1) Riess, G. Micellization of block copolymers. *Prog. Polym. Sci.* **2003**, *28*, 1107−1170.

(2) Mai, Y.; Eisenberg, A. Self-assembly of block copolymers. *Chem. Soc. Rev.* **2012**, *41*, 5969−5985.

(3) Sarkar, B.; Alexandridis, P. Block copolymer−nanoparticle composites: Structure, functional properties, and processing. *Prog. Polym. Sci.* **2015**, *40*, 33−62.

(4) Kim, H.; Park, S.; Hinsberg, W. D. Block Copolymer Based Nanostructures: Materials, Processes, and Applications to Electronics. *Chem. Rev.* **2010**, *110*, 146−177.

(5) Mokarian-Tabari, P.; Senthamaraikannan, R.; Glynn, C.; Collins, T. W.; Cummins, C.; Nugent, D.; O'Dwyer, C.; Morris, M. A. Large block copolymer self-assembly for fabrication of subwavelength nanostructures for applications in optics. *Nano Lett.* **2017**, *17*, 2973−2978.

(6) Li, Z.; Loh, X. J. Water soluble polyhydroxyalkanoates: future materials for therapeutic applications. *Chem. Soc. Rev.* **2015**, *44*, 2865−2879.

(7) Sen, D.; Das, A.; Kumar, A.; Bahadur, J.; Chaurasia, R. K.; Khan, A.; Ganguly, R. Amphiphilic interaction-mediated ordering of nanoparticles in Pickering emulsion droplets. *Soft Matter* **2023**, *19*, 3953−3965.

(8) Zheng, R.; Binks, B. P.; Cui, Z. G. Pickering emulsions of hydrophilic silica particles and symmetrical organic electrolytes. *Langmuir* **2020**, *36*, 4619−4629.

(9) Xue, Y.; Li, X.; Dong, J. Interfacial characteristics of block copolymer micelles stabilized Pickering emulsion by confocal laser scanning microscopy. *J. Colloid Interface Sci.* **2020**, *563*, 33−41.

(10) Xue, Y.; Dong, J.; Li, X. Fabricating switchable Pickering emulsions by dynamic covalent copolymer amphiphiles. *Colloids Surf., A* **2023**, *656*, 130399.

(11) He, X.; Xue, Y.; Dong, J.; Li, X. Multiple Pickering emulsions fabricated by a single block copolymer amphiphile in one-step. *Colloids Surf., A* **2023**, *657*, 130557.

(12) Hunter, S. J.; Armes, S. P. Pickering Emulsifiers Based on Block Copolymer Nanoparticles Prepared by Polymerization-Induced Self-Assembly. *Langmuir* **2020**, *36*, 15463−15484.

(13) Zhang, T.; Jiang, H.; Hong, L.; Ngai, T. Multiple Pickering emulsions stabilized by surface-segregated micelles with adaptive wettability. *Chem. Sci.* **2022**, *13*, 10752−10758.

(14) Tang, J.; Quinlan, P. J.; Tam, K. C. Stimuli-responsive Pickering emulsions: recent advances and potential applications. *Soft Matter* **2015**, *11*, 3512−3529.

(15) Keddie, D. J. A guide to the synthesis of block copolymers using reversible-addition fragmentation chain transfer (RAFT) polymerization. *Chem. Soc. Rev.* **2014**, *43*, 496−505.

(16) Ran, J.; Wu, L.; Zhang, Z.; Xu, T. Atom transfer radical polymerization (ATRP): A versatile and forceful tool for functional membranes. *Prog. Polym. Sci.* **2014**, *39*, 124−144.

(17) Sciannamea, V.; Jérôme, R.; Detrembleur, C. In-situ nitroxide-mediated radical polymerization (NMP) processes: their understanding and optimization. *Chem. Rev.* **2008**, *108*, 1104−1126.

(18) Rieger, J. Guidelines for the Synthesis of Block Copolymer Particles of Various Morphologies by RAFT Dispersion Polymerization. *Macromol. Rapid Commun.* **2015**, *36*, 1458−1471.

(19) Lowe, A. B. RAFT alcoholic dispersion polymerization with polymerization-induced self-assembly. *Polymer* **2016**, *106*, 161−181.

(20) Sun, J. T.; Hong, C. Y.; Pan, C. Y. Recent advances in RAFT dispersion polymerization for preparation of block copolymer aggregates. *Polym. Chem.* **2013**, *4*, 873−881.

(21) Canning, S. L.; Smith, G. N.; Armes, S. P. A critical appraisal of RAFT-mediated polymerization-induced self-assembly. *Macromolecules* **2016**, *49*, 1985−2001.

(22) Charleux, B.; Delaittre, G.; Rieger, J.; D'Agosto, F. Polymerization-induced self-assembly: from soluble macromolecules to block

copolymer nano-objects in one step. *Macromolecules* **2012**, *45*, 6753−6765.
(23) Derry, M. J.; Fielding, L. A.; Armes, S. P. Polymerization-induced self-assembly of block copolymer nanoparticles via RAFT non-aqueous dispersion polymerization. *Prog. Polym. Sci.* **2016**, *52*, 1−18.
(24) Figg, C. A.; Simula, A.; Gebre, K. A.; Tucker, B. S.; Haddleton, D. M.; Sumerlin, B. S. Polymerization-induced thermal self-assembly (PITSA). *Chem. Sci.* **2015**, *6*, 1230−1236.
(25) Figg, C. A.; Carmean, R. N.; Bentz, K. C.; Mukherjee, S.; Savin, D. A.; Sumerlin, B. S. Tuning hydrophobicity to program block copolymer assemblies from the inside out. *Macromolecules* **2017**, *50*, 935−943.
(26) Liu, T.; Xue, F.; Yi, P.; Xia, Z.; Dong, J.; Li, X. F. Structure−property relationship of light-responsive wormlike micelles using methoxycinnamate derivatives as light-switchable molecules. *Acta Phys.-Chim. Sin.* **2020**, *36*, 1910004.
(27) Zhao, W.; Gody, G.; Dong, S.; Zetterlund, P. B.; Perrier, S. Optimization of the RAFT polymerization conditions for the in situ formation of nano-objects via dispersion polymerization in alcoholic medium. *Polym. Chem.* **2014**, *5*, 6990−7003.
(28) Sugihara, S.; Blanazs, A.; Armes, S. P.; Ryan, A. J.; Lewis, A. L. Aqueous dispersion polymerization: A new paradigm for in situ block copolymer self-assembly in concentrated solution. *J. Am. Chem. Soc.* **2011**, *133*, 15707−15713.
(29) Israelachvili, J. N.; Mitchell, D. J.; Ninham, B. W. Theory of self-assembly of hydrocarbon amphiphiles into micelles and bilayers. *J. Chem. Soc., Faraday Trans.* **1976**, *72*, 1525−1568.
(30) Blanazs, A.; Ryan, A. J.; Armes, S. P. Predictive phase diagrams for RAFT aqueous dispersion polymerization: Effect of block copolymer composition, molecular weight, and copolymer concentration. *Macromolecules* **2012**, *45*, 5099−5107.
(31) Fielding, L. A.; Lane, J. A.; Derry, M. J.; Mykhaylyk, O. O.; Armes, S. P. Thermo-responsive diblock copolymer worm gels in non-polar solvents. *J. Am. Chem. Soc.* **2014**, *136*, 5790−5798.
(32) Derry, M. J.; Fielding, L. A.; Warren, N. J.; Mable, C. J.; Smith, A. J.; Mykhaylyk, O. O.; Armes, S. P. In situ small-angle X-ray scattering studies of sterically-stabilized diblock copolymer nanoparticles formed during polymerization-induced self-assembly in non-polar media. *Chem. Sci.* **2016**, *7*, 5078−5090.
(33) Zhang, J. P.; Zou, M.; Dong, J. F.; Li, X. F. Synthesis and self-assembly behaviors of well-defined poly(lauryl methacrylate)-block-poly[N-(2-methacryloylxyethyl)pyrrolidone] copolymers. *Colloid Polym. Sci.* **2013**, *291*, 2653−2662.
(34) Zhang, J. P.; Cheng, S. Z.; Li, X. F.; Dong, J. F. pH- and temperature-induced micellization of the dual hydrophilic block copolymer poly(methacrylate acid)-b-poly(N-(2-methacryloylxyethyl) pyrrolidone) in aqueous solution. *Acta Phys.-Chim. Sin.* **2016**, *32*, 2018−2026.
(35) Cheng, S. Z.; Xue, Y.; Lu, Y. C.; Li, X. F.; Dong, J. F. Thermoresponsive pyrrolidone block copolymer organogels from 3D micellar networks. *ACS Omega* **2017**, *2*, 105−112.
(36) Cunningham, V. J.; Armes, S. P.; Musa, O. M. Synthesis, characterisation and Pickering emulsifier performance of poly-(stearylmethacrylate)−poly(N-2-(methacryloyloxy)ethyl pyrrolidone) diblock copolymer nano-objects via RAFT dispersion polymerisation in n-dodecane. *Polym. Chem.* **2016**, *7*, 1882−1891.
(37) Cunningham, V. J.; Derry, M. J.; Fielding, L. A.; Musa, O. M.; Armes, S. P. RAFT aqueous dispersion polymerization of N-(2-(methacryloyloxy)ethyl)pyrrolidone: A convenient low viscosity route to high molecular weight water-soluble copolymers. *Macromolecules* **2016**, *49*, 4520−4533.
(38) Cunningham, V. J.; Ning, Y.; Armes, S. P.; Musa, O. M. Poly(N-2-(methacryloyloxy)ethyl pyrrolidone)-poly(benzyl methacrylate) diblock copolymer nano-objects via RAFT alcoholic dispersion polymerisation in ethanol. *Polymer* **2016**, *106*, 189−199.
(39) Cao, C.; Chen, F.; Garvey, C. J.; Stenzel, M. H. Drug-directed morphology changes in polymerization-induced self-assembly (PISA) influence the biological behavior of nanoparticles. *ACS Appl. Mater. Interfaces* **2020**, *12*, 30221−30233.
(40) Pearce, S.; Perez-Mercader, J. PISA: construction of self-organized and self-assembled functional vesicular structures. *Polym. Chem.* **2021**, *12*, 29−49.
(41) Brotherton, E. E.; Hatton, F. L.; Cockram, A. A.; Derry, M. J.; Czajka, A.; Cornel, E. J.; Topham, P. D.; Mykhaylyk, O. O.; Armes, S. P. In situ small-angle X-ray scattering studies during reversible addition−fragmentation chain transfer aqueous emulsion polymerization. *J. Am. Chem. Soc.* **2019**, *141*, 13664−13675.
(42) Liu, C.; Hong, C. Y.; Pan, C. Y. Polymerization techniques in polymerization-induced self-assembly (PISA). *Polym. Chem.* **2020**, *11*, 3673−3689.
(43) Fielding, L. A.; Derry, M. J.; Ladmiral, V.; Rosselgong, J.; Rodrigues, A. M.; Ratcliffe, L. P. D.; Sugihara, S.; Armes, S. P. RAFT dispersion polymerization in non-polar solvents: facile production of block copolymer spheres, worms and vesicles in n-alkanes. *Chem. Sci.* **2013**, *4*, 2081−2087.
(44) Canning, S. L.; Cunningham, V. J.; Ratcliffe, L. P. D.; Armes, S. P. Phenyl acrylate is a versatile monomer for the synthesis of acrylic diblock copolymer nano-objects via polymerization-induced self-assembly. *Polym. Chem.* **2017**, *8*, 4811−4821.
(45) Xu, X. F.; Zhu, R. M.; Pan, C. Y.; You, Y. Z.; Zhang, W. J.; Hong, C. Y. Polymerization-induced self-assembly driven by the synergistic effects of aromatic and solvophobic interactions. *Macromolecules* **2021**, *54*, 2729−2739.

https://doi.org/10.1021/acsomega.3c09315
ACS Omega 2024, 9, 36917−36925